CBN 02-9
CBX 02-33
September 2002
D. Cinabro
K. Korbiak

Techniques to Measure CESR Beam Parameters: β_x^*, ϵ_x, ϵ_y, $\frac{\Delta \mathrm{E}}{\mathrm{E}_{\mathrm{beam}}}$

Abstract

We have developed techniques that allow simultaneous measurements of the spatial size of the luminous region and the angular spread of the $e^+e^- \to \mu^+\mu^-$ events from the CLEO interaction point of CESR which is related to the angular spread of the colliding beams. These techniques take advantage of the small and well understood resolution of the CLEO II.V tracking system. We use these measurements to extract the horizontal beta, horizontal emittance and the vertical emittance as functions of specific luminosity and beam current. We also set limits on the beam energy spread in the CLEO II.V dataset.

1 Introduction

Emboldened by at least two recent examples showing that, for high momentum tracks, the simulation of the tracking in CLEO II.V accurately models the data [1] [2], we use the fact that we know the momentum resolution to $\pm 4\%$ to try to measure the horizontal and vertical emittance of the CESR beam. The basic technique will be to select $e^+e^- \to \mu^+\mu^-$ events, measure the total momentum of the two observed tracks, and unfold from this the contribution from the momentum resolution of the CLEO II.V tracking system and the underlying difference caused by the angular spread or mismatched energy of the beam particles. Combining the angular spread of the beam with the spatial spread of the beam, measured with the box method [2], we can simultaneously extract the beam parameters, beta star and emittance. By considering the data as a function of beam current and of specific luminosity, defined as the average luminosity over beam current, we can search for dynamic changes of emittance.

The shape of a beam in the interaction region is described elsewhere [2][3]. The relevant parameters are β_x^*, the horizontal beta function at the CESR–CLEO collision point, β_y^*, the vertical beta function at the CESR–CLEO collision point, ϵ_x, the horizontal emittance, ϵ_y, the vertical emittance. If dispersion at the interaction point and coupling are negligible, these parameters are related to the physical observables σ, the Gaussian width of the spatial spread of the beam, and σ', the Gaussian width of the angular spread of the beam, by the following equations:

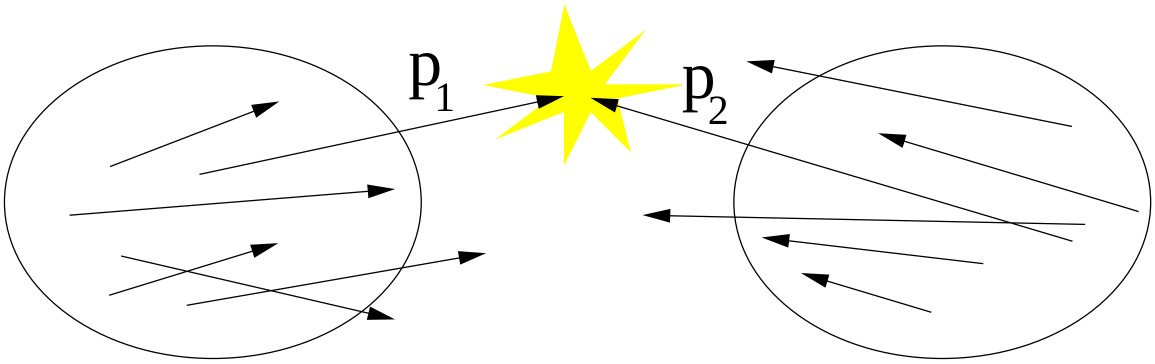

Figure 1: Particles in the beam do not collide head on, but at some angle. The width of this angular distribution, or the angular spread, is $\sigma\mathcal{L}'$.

$$\sigma_x = \sqrt{\beta_x^* \epsilon_x} \quad (1)$$
$$\sigma_y = \sqrt{\beta_y^* \epsilon_y} \quad (2)$$
$$\sigma_x' = \sqrt{\epsilon_x / \beta_x^*} \quad (3)$$
$$\sigma_y' = \sqrt{\epsilon_y / \beta_y^*}. \quad (4)$$

A simultaneous measurement of σ and σ' in the collision region would yield measurements of β^* and ϵ via the obvious algebraic manipulation. This simultaneous measurement is possible using the method described below.

The spatial spread, of the luminous region is measured using the box method, already used in our hourglass observation [2], and a new technique is used to measure the angular spread of the beam. These are related to the spatial width of the luminous region, $\sigma_{\mathcal{L}} = \sigma/\sqrt{2}$, as well as to the angular width of the $\mu^+\mu^-$ pairs produced by the collision of the two beams, $\sigma'_{\mathcal{L}} = \sqrt{2}\sigma'$.

The effect of the angular spread of the approaching beams in CESR is depicted in the diagram shown in Figure 1. As the beams collide, the particles do not interact head on, but at some non-trivial angle to one another. This gives rise to a distribution, of non-zero width, of the angle between the two tracks in $e^+e^- \to \mu^+\mu^-$ even before a finite resolution is taken into account.

The beam parameters for CESR during the 4ST running period, October 1998 through February 1999, on the 4S are given in Table 1. Note that all the parameters in Table 1 are given at zero beam current. We expect to observe small dynamic effects for β_y^*, while there is a significant dependence on the beam current for β_x^*. A reduction of approximately two is expected, based on these previous results [4]. Dynamic effects are expected to give a small reduction in ϵ_x. On the other hand, ϵ_y is dominated by beam-beam dynamic effects. We can constrain it using the observed luminosity and by doing so predict a range from 0.001 to 0.010 μm-rad. The goal of this work, nonetheless, is the search for any dynamic effects of the horizontal and vertical emittances.

Table 1: CESR beam parameters at zero beam current during the 4ST running period for on 4S running.

Parameter	Value (μm)
β_x^*	1.1996×10^6
β_y^*	17900
ϵ_x	0.21
ϵ_y	0.0010

2 Method

To ensure the best resolution on the luminous region, $e^+e^- \to \mu^+\mu^-$ events are chosen using `KLASGL = 6`[5], `NTRKCD = 2`. Both tracks must have more than 20 CD hits, at least two SVX hits in the $r\phi$ and z views, and not be a DREDGE or ZESCAPE. The tracks must have at least three SVX hits in one of the two views. They must also be of opposite charge. Each point for measuring σ'_x is based roughly on 7000 events; for σ'_y 2000 events.

To measure the angle between two colliding tracks, we first divide the sum of the momenta of the two tracks by the beam energy. We call this the peculiar momentum. We take into account the crossing angle by subtracting the run-by-run measured crossing angle from the peculiar momentum. With this correction, the means of the peculiar momenta are consistent with zero. This corrected peculiar momentum is equivalent to the minor arc between the colliding tracks. The minor arc is given by $\sin\theta$, where θ is the central angle between the colliding tracks. For small angles we use the approximation $\sin\theta \approx \theta$. Thus the small angle between the two tracks in the horizontal and vertical directions is determined. This method is schematically shown in Figure 2. The width of the distribution of the angles between tracks is related to the width of the angular distribution of the beam, σ'.

The key to this method is knowing the resolution on the central angle. We study this with a simulated sample of $e^+e^- \to \mu^+\mu^-$ events generated with no momentum spread in the incoming beam particles. We guessed that the resolution on the central angle would depend on global properties of the event rather than the properties of the two individual tracks. In the angle analysis, the direction cosines were restricted to $|\cos\theta_y| < 0.1$ to effectively measure the vertical luminous region, a looser cut of $|\cos\theta_x| < 0.3$ for the horizontal. We also restricted the longitudinal direction cosine by making the cut $|\cos\theta_z| < 0.7$. We must also restrict the data to the region where the hourglass effect [2] does not cause the resolution to increase. The hourglass effect causes tightly focused beams to have a "waist" at the focal point of the final quadrupoles. The size of these beams grows away from this waist, therefore we make a cut on the longitudinal position, $|\text{zpos}| < 0.5$cm. We also guessed that the number and source of SVX hits on the two tracks would lead to different resolutions, thus we broke our sample into those with six $r\phi$ and six z hits (6,6), six $r\phi$ and five z hits (6,5), etc. SVX hit patterns on the two tracks. For each of these sub samples we parametrized the resolution as

$$A/Nhits + B = \sigma_N \tag{5}$$

where $Nhits$ is the total number of tracking hits in the SVX, VD, and DR used on both tracks. To determine A and B for each SVX hit pattern we fit the two dimensional distribution of central

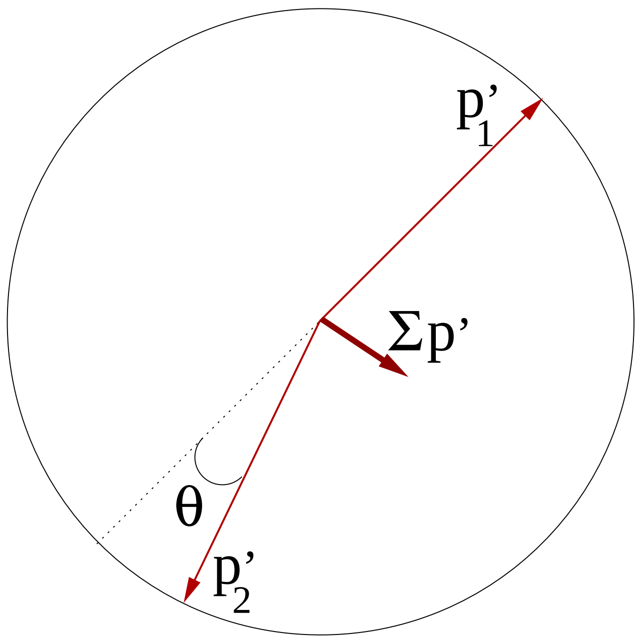

Figure 2: The peculiar momentum of the two tracks is obtained by taking the sum of the momenta of two tracks and dividing by the beam energy. This defines an angle which is the central angle, θ, giving the minor arc, $\sin\theta$. The minor arc defined by θ is equivalent to the peculiar momentum of the two tracks.

Table 2: Parameters of the resolution on the central angle in $e^+e^- \to \mu^+\mu^-$ events. They are determined as described in the text. The resolution as a function of the total number of tracking hits for each case is given by $\sigma_N = A/Nhits + B$.

Direction	SVX Hit Pattern $(r\phi, z)$	A (rad–hit)	B (rad$\times 10^4$)
Horizontal	(6,6)	0.255±0.020	-6.8±1.8
Horizontal	(6,5)	0.226±0.036	-3.6±3.2
Horizontal	(5,6)	0.073±0.041	11.0±3.6
Vertical	(6,5)	0.135±0.020	-3.6±2.4
Vertical	(6,4)	0.093±0.026	0.3±1.4

angle versus $Nhits$, in each bin of $Nhits$, to a Gaussian with a width given by σ_N plus a flat background. To display the results of this fit, we show the width of the resolution as a function of $Nhits$, determined by selecting on a range of $Nhits$ and performing a one dimensional fit to a Gaussian plus a flat background. In Figures 3, 4, 5, 6 and 7 we compare the results of this one dimensional fit to the result for σ_N for each SVX hit pattern and for vertical and horizontal directions. These Figures show that our parameterization of the resolution on the central angle is a reasonable match to the prediction of the simulation. Table 2 summarizes the results of the parameterization. SVX hit patterns that do not appear are not used either due to limited statistics in the simulated or real data. We require more than 100 entries in each plot to fit. For the position analysis, we use the same technique as in the hourglass analysis, including also the $|\text{zpos}| < 0.5$cm cut.

To extract $\sigma'_{\mathcal{L}}$ for each bin of $Nhits$ corresponding to a given SVX hit pattern, we fit to a Gaussian with a width given by

$$\sqrt{(A/Nhits + B)^2 + \sigma'^2_{\mathcal{L}}}. \tag{6}$$

In these fits, A and B are fixed and the area, mean, $\sigma'_{\mathcal{L}}$, and a flat background are floating. We then form a weighted average of the $\sigma'_{\mathcal{L}}$, for all SVX hit patterns and $Nhits$ bins for a given range of beam current or specific luminosity.

Finally, the horizontal β^* and ϵ are expected to be functions primarily of the beam current, while the vertical ϵ is expected to be influenced more by the specific luminosity. Therefore we present measurements in the horizontal direction as functions of beam current, while measurements in the vertical are presented as functions of specific luminosity.

3 Results

The measured horizontal and vertical Gaussian width of the luminous region are shown in Figures 8 and 9, respectively. We measure an average horizontal width of the luminous region of approximately 300 μm, in full agreement with our previous results in the hourglass work [2]. However, the average measured vertical width is much wider than the expected width of approximately 8 μm. Thus we are not measuring the vertical width, but the resolution on the position. We take σ_y to be the resolution on the position, hence we are not able to measure β^*_y.

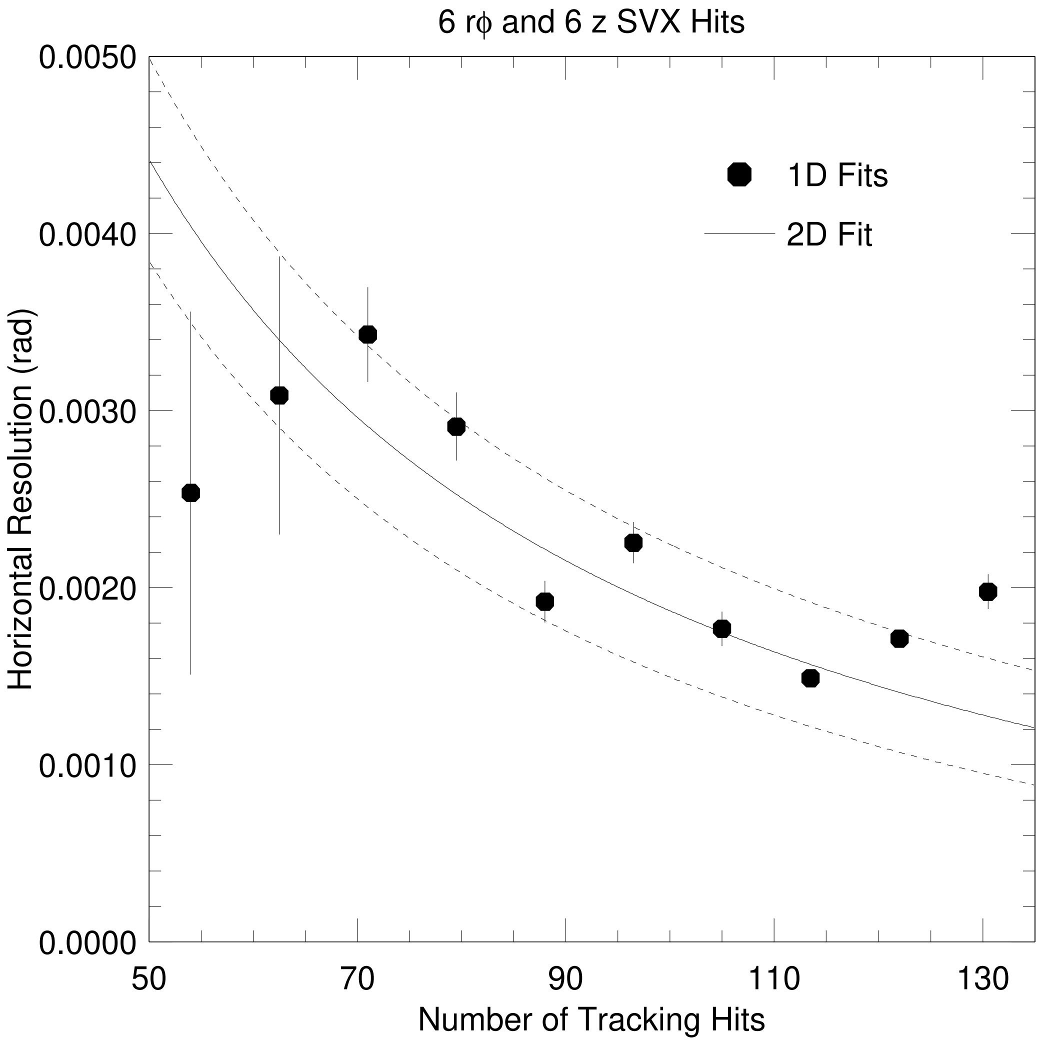

Figure 3: For the horizontal central angle, the resolution in $e^+e^- \to \mu^+\mu^-$ with an SVX hit pattern of ($6\ r\phi$,$6\ z$) as a function of the total number of tracking hits on both tracks as predicted by the simulation. Also shown is the resolution parametrized as $A/Nhits + B$ with the central value as a full line and the dashed lines showing the one standard deviation uncertainty due the errors on the A and B parameters.

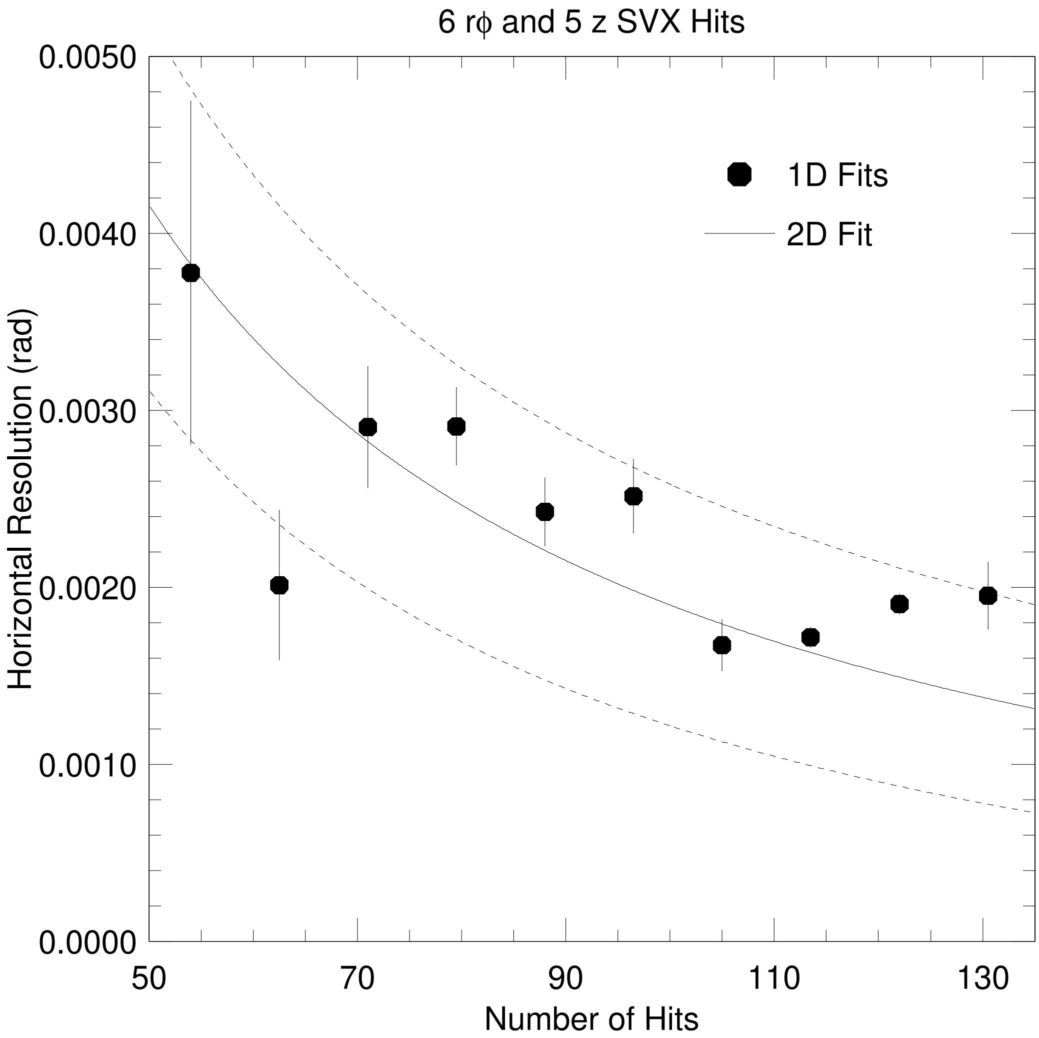

Figure 4: For the horizontal central angle, the resolution in $e^+e^- \to \mu^+\mu^-$ events with an SVX hit pattern of (6 $r\phi$,5 z) as a function of $Nhits$ as predicted by the simulation. Also shown is the resolution parametrized as $A/Nhits + B$ with the central value as a full line and the dashed lines showing the one standard deviation uncertainty due the errors on the A and B parameters.

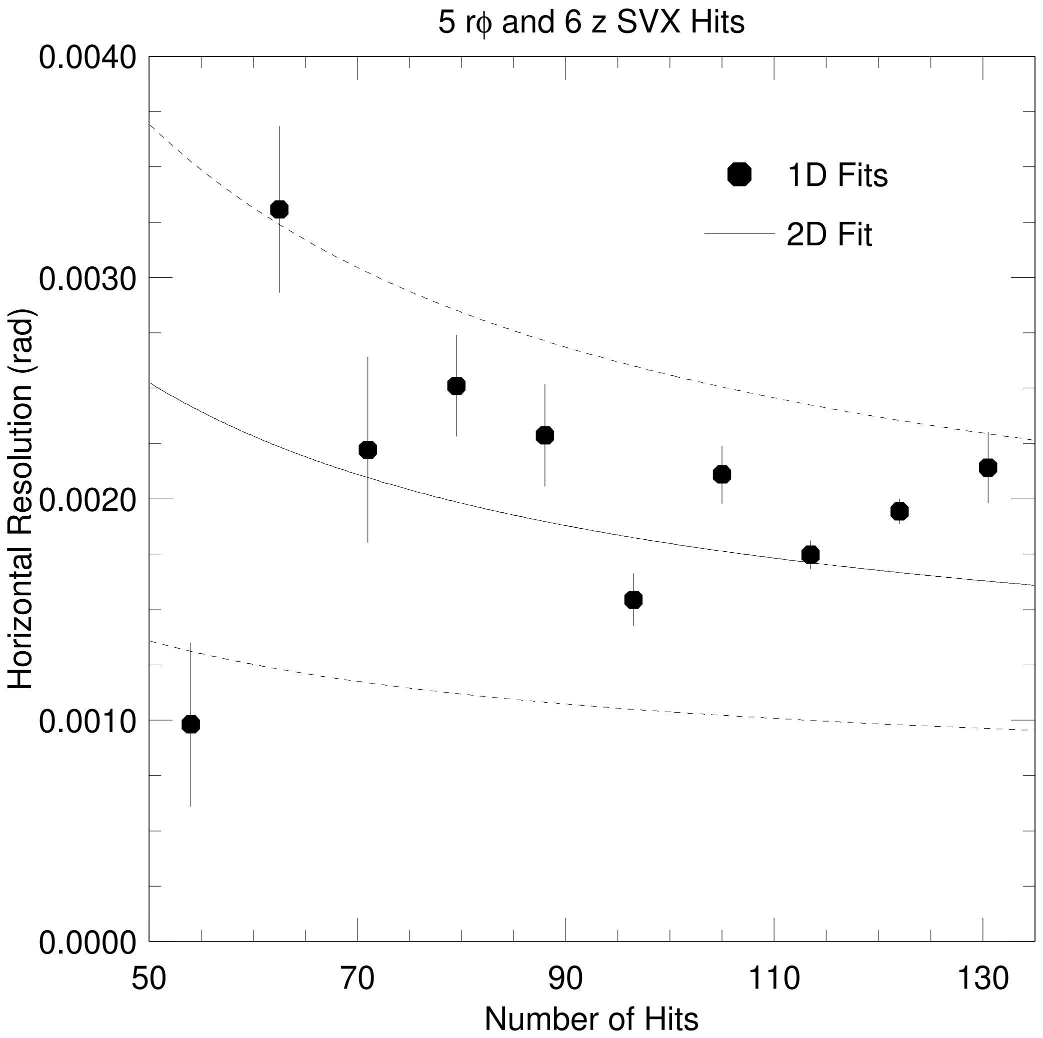

Figure 5: For the horizontal central angle, the resolution in $e^+e^- \rightarrow \mu^+\mu^-$ events with an SVX hit pattern of (5 $r\phi$,6 z) as a function of $Nhits$ as predicted by the simulation. Also shown is the resolution parametrized as $A/Nhits + B$ with the central value as a full line and the dashed lines showing the one standard deviation uncertainty due the errors on the A and B parameters.

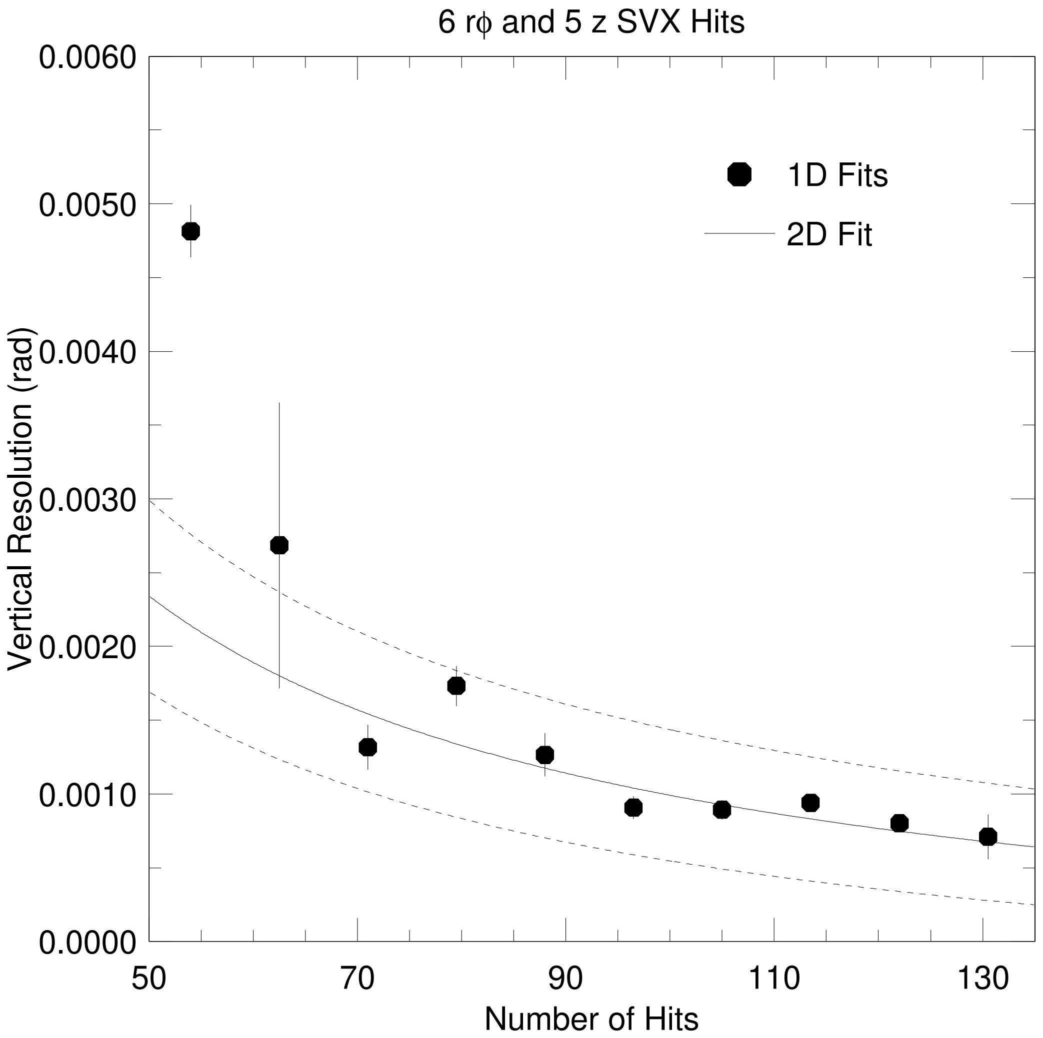

Figure 6: For the vertical central angle, the horizontal resolution in $e^+e^- \rightarrow \mu^+\mu^-$ events with an SVX hit pattern of (6 $r\phi$,5 z) as a function of $Nhits$ as predicted by the simulation. Also shown is the resolution parametrized as $A/Nhits + B$ with the central value as a full line and the dashed lines showing the one standard deviation uncertainty due the errors on the A and B parameters.

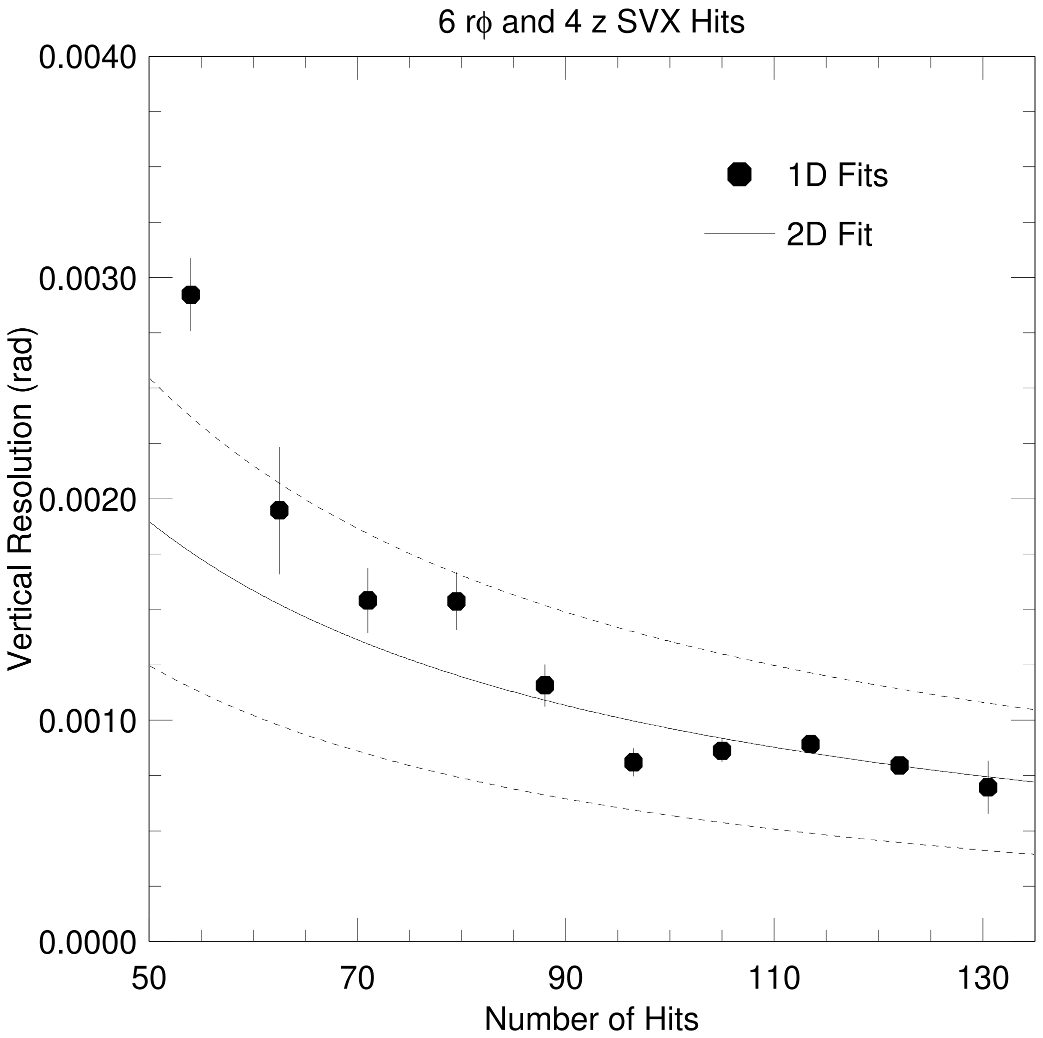

Figure 7: For the vertical central angle, the horizontal resolution in $e^+e^- \to \mu^+\mu^-$ events with an SVX hit pattern of (6 $r\phi$,4 z) as a function of $Nhits$ as predicted by the simulation. We again show the resolution parametrized as $A/Nhits + B$ with the central value as a full line and the dashed lines showing the one standard deviation uncertainty due the errors on the A and B parameters.

In the hourglass work [2] we measure a constant $\beta_y^* = 17910 \pm 170\mu$m and this value is used later to extract ϵ_y.

The width of the horizontal angular distribution of the luminous region, as a function of the beam current, is displayed in Figure 10. To be clear we are displaying the extracted underlying width after taking into account the resolution with the fits described above. If the luminous region has no underlying width, the expected width of the angular distribution would be approximately 2.0 mrad, as seen in the resolution model discussed in the previous section. We observe a raw horizontal width approximately 15% wider. We attribute this discrepancy to an underlying width of the luminous region due to emittance. Figure 11 shows the intrinsic vertical angular distribution in the luminous region as a function of specific luminosity. The resolution in the vertical direction is better, approximately 1.5 mrad. Here we see only a 10% increase over 1.5 mrad in the width of the angular distribution. Thus measuring in the vertical direction is more difficult, leading to larger uncertainty.

We now use the simultaneous measurements of σ_x, σ'_x and σ'_y to extract the beam parameters β_x^*, ϵ_x and ϵ_y. Recall that we do not measure β_y^*, but use a constant value of 17910$\pm$170 μm to extract ϵ_y. The extracted β_x^* is shown in Figure 12. This result agrees well with our expectations based on a previous analysis done on dynamic beta [4]. The expectation was $\beta_x^* = 1.2$m reduced by roughly a factor of two. Here we see a $\beta_x^* \approx 0.6$m agreeing well with the expectation. The extracted horizontal emittance is displayed in Figure 13. We expected an $\epsilon_x = 0.21\mu$m-rad while we extracted an $\epsilon_x \approx 0.3\mu$m. These results again agree well with our expectation. We also expected little dynamic effects. Here we clearly do not see any dynamic effects. We also expect an extracted vertical emittance in the range $\epsilon_y = 0.0100 - 0.0010\mu$m-rad. We extract an $\epsilon_y \approx 0.0030\mu$m-rad, which is within the range of our expectation. Moreover, our extracted value agrees with an earlier observation of $\epsilon_y = (0.0070 \pm 0.0054 \pm 0.0019)\mu$m-rad [2]. This extracted vertical emittance, shown in Figure 14 appears to have dynamic effects. When a χ^2 fit to a first order polynomial is applied to this data, a slope of 2.13$\pm$0.90 is observed. This is less than three standard deviations from zero and thus is not significant. Therefore there are no visible dynamic effects on vertical emittance.

We also do a study of the systematic error associated with the analysis. We repeated the fits using the maximum and minimum A and B values, as determined by the errors on A and B. Using these values, we again extract β_x^*, ϵ_x and ϵ_y as functions of specific luminosity. The resulting plots have the same shape as those presented above, but are shifted upward or downward. Using this data, we determined the systematic error on β_x^* to be $(+0.15 - 0.10)$m, $(\pm 0.07)\mu$m-rad on ϵ_x, and $(\pm 0.002)\mu$m-rad on ϵ_y. We also studied the effect of using only bins with $Nhits > 90$. The effect of this cut is negligible. Bins of $Nhits < 90$ generally have low statistics and very few are actually considered in the analysis.

By considering the week ending January 7, 1999, when the machine performed best during this running period, we made a cross check on this technique. Using the known horizontal dynamic beta effects and the equation

$$\mathcal{L} = \frac{f \mathrm{N_e} \mathrm{N_p}}{4\pi\sigma_x\sigma_y}, \tag{7}$$

where $\mathcal{L}$ is the luminosity, f is the frequency of collisions, $\mathrm{N_e}$ is the number of electrons, $\mathrm{N_p}$ is the number of positrons, and σ_x and σ_y are the horizontal and vertical beam sizes, we are able to calculate expectations for β_x^*, ϵ_x and ϵ_y. We use the measured luminosity of $7.2 \times 10^{32}/\mathrm{cm}^2\mathrm{sec}$

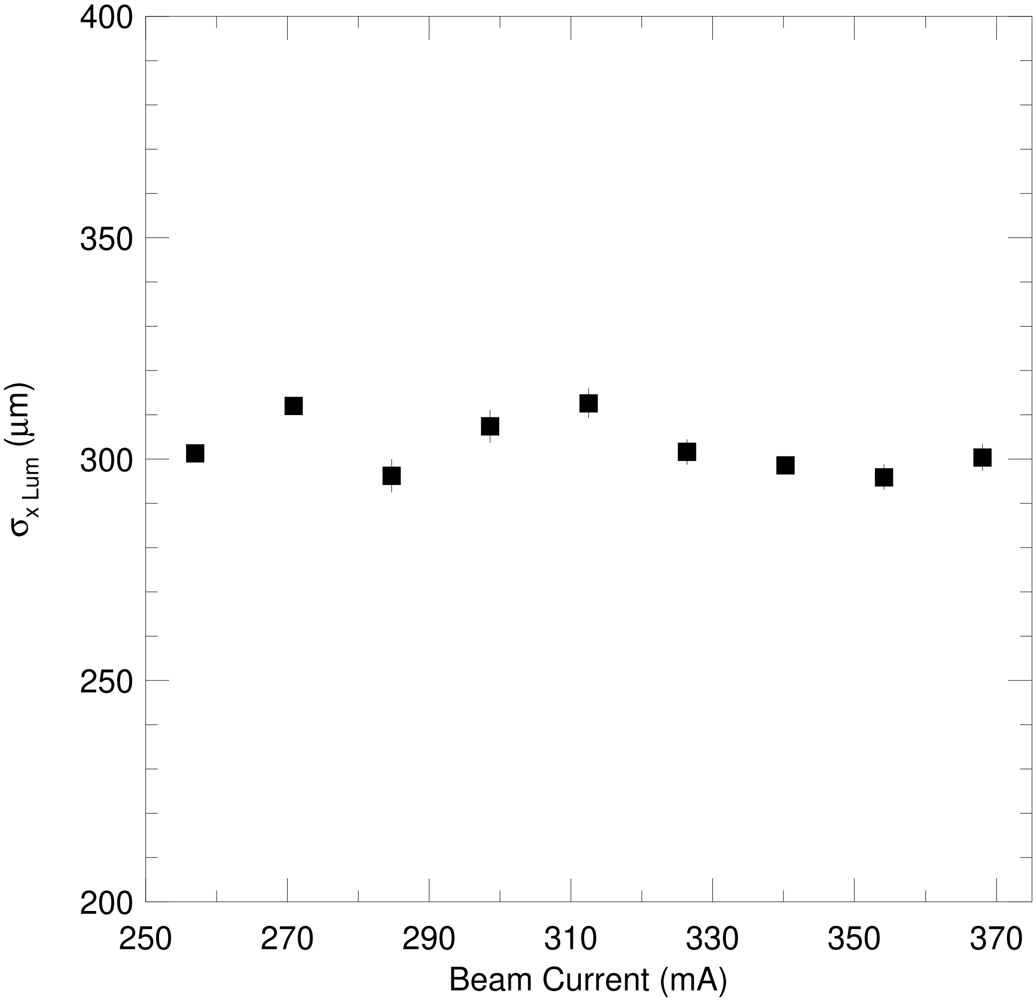

Figure 8: The Gaussian width of the horizontal luminous region as a function of beam current.

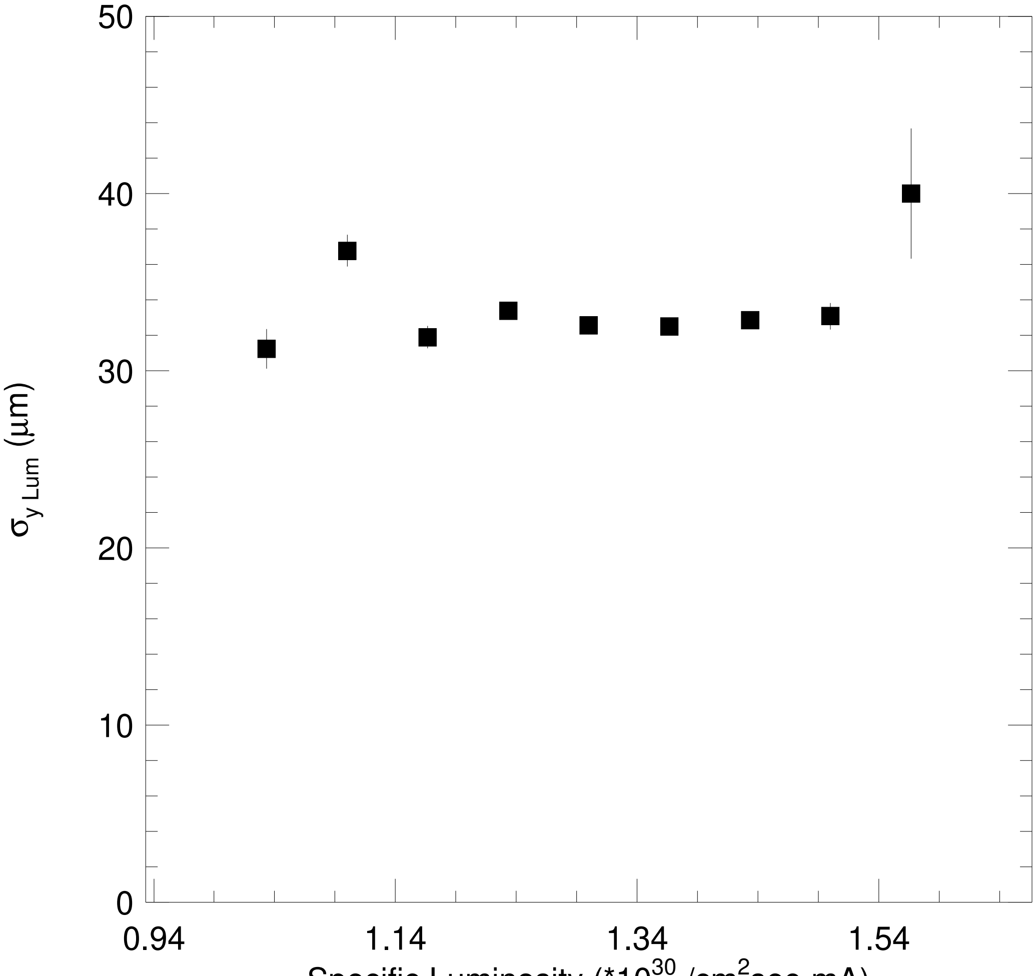

Figure 9: The Gaussian width of the vertical luminous region as a function of specific luminosity.

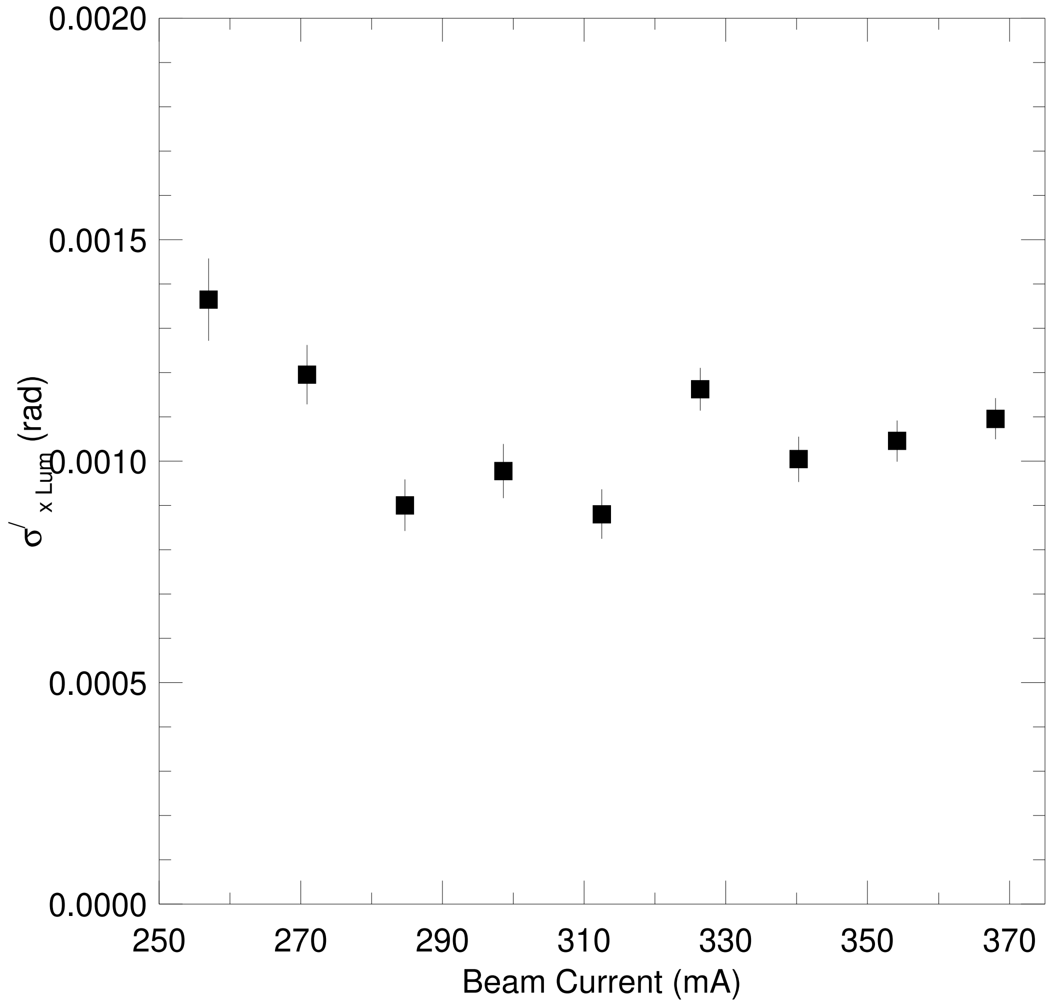

Figure 10: The intrinsic width of the horizontal angular distribution of the luminous region as a function of beam current.

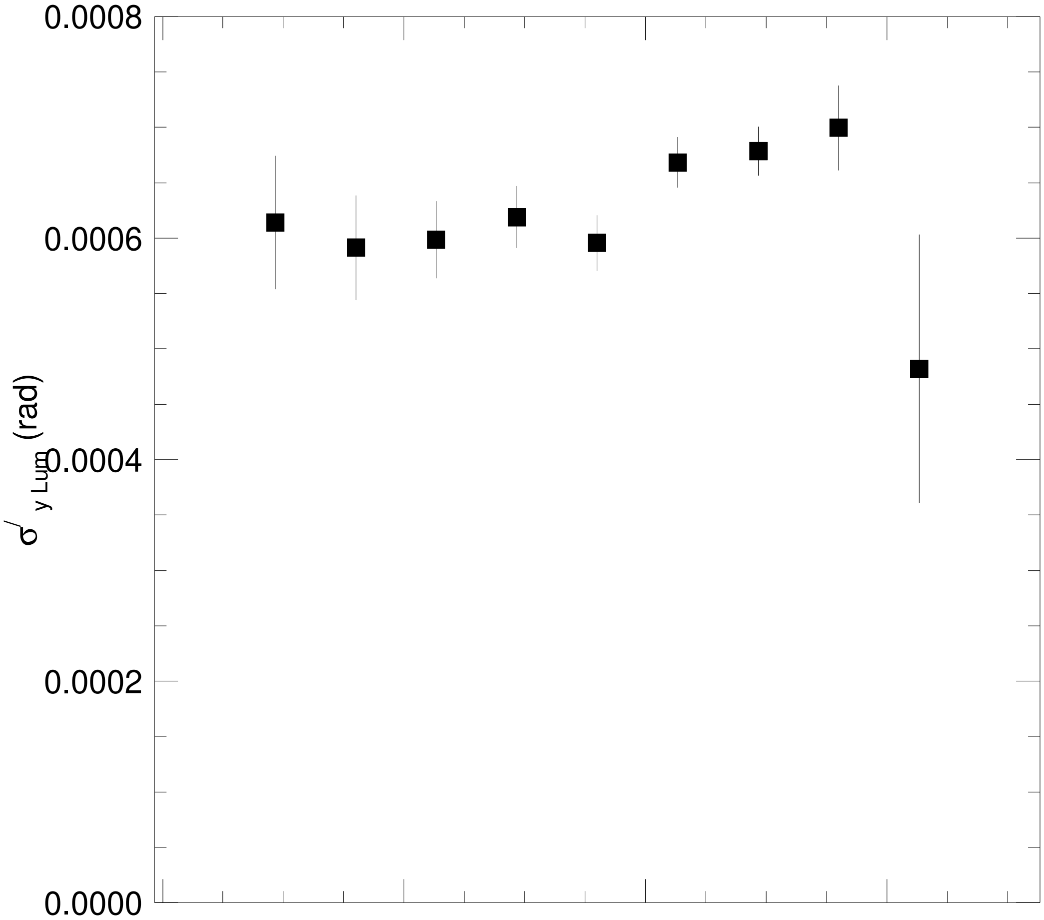

Figure 11: The intrinsic width of the vertical angular distribution of the luminous region as a function of specific luminosity.

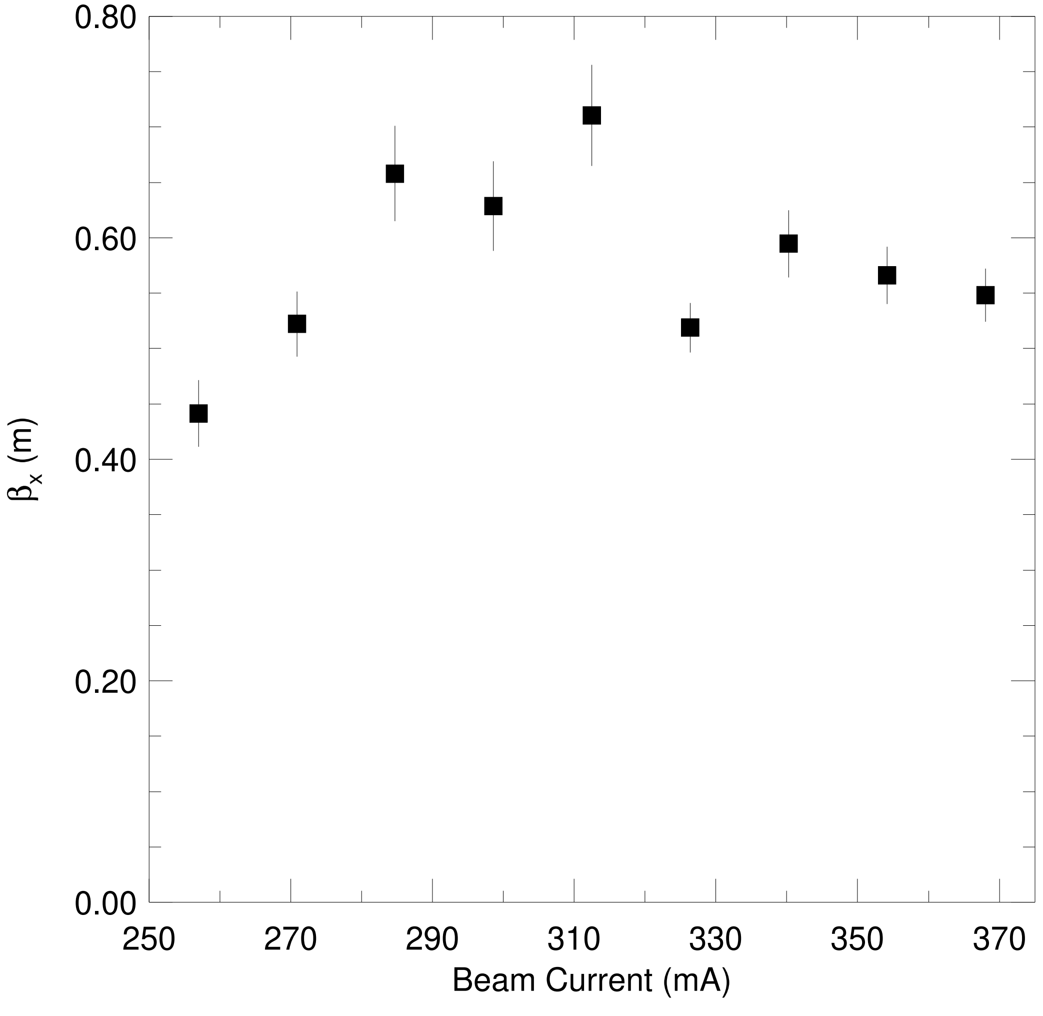

Figure 12: The extracted horizontal beta as a function of beam current.

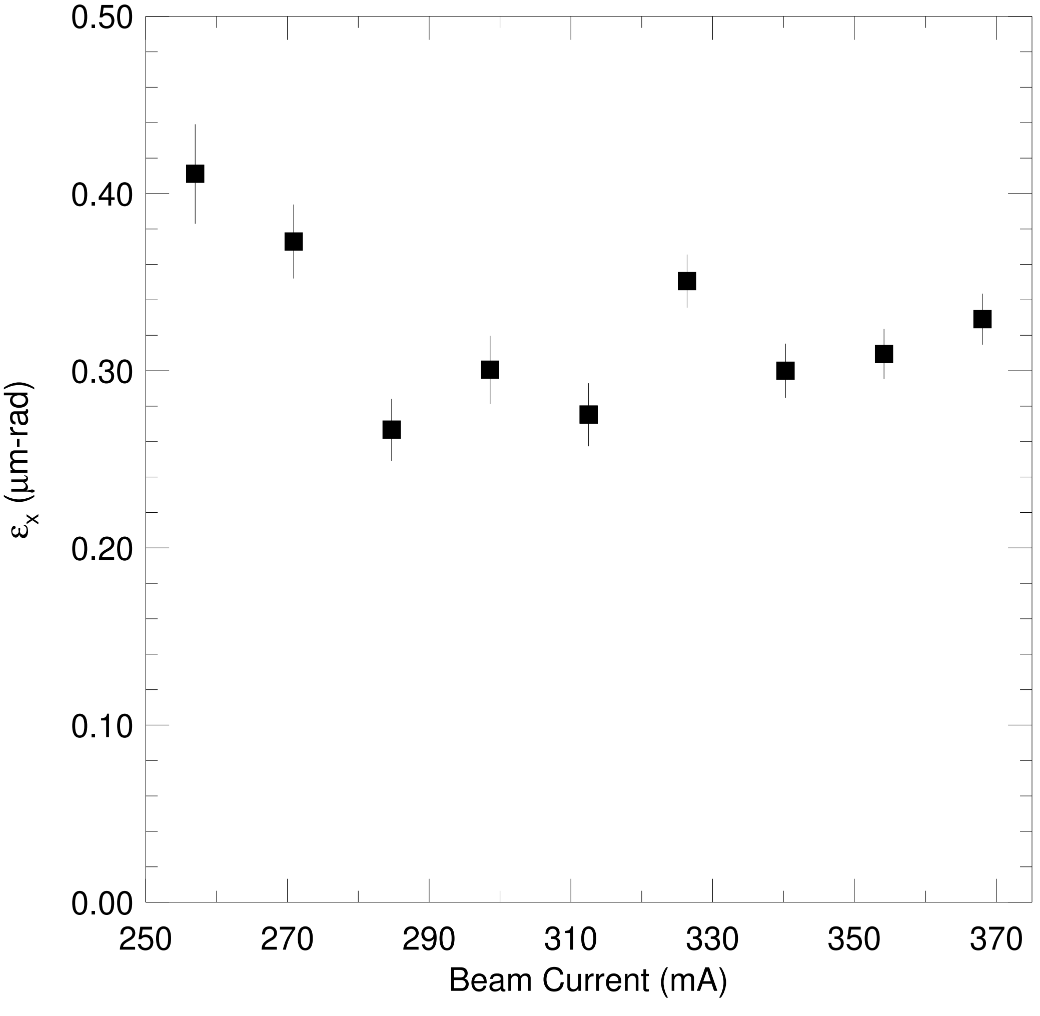

Figure 13: The extracted horizontal emittance as a function of beam current.

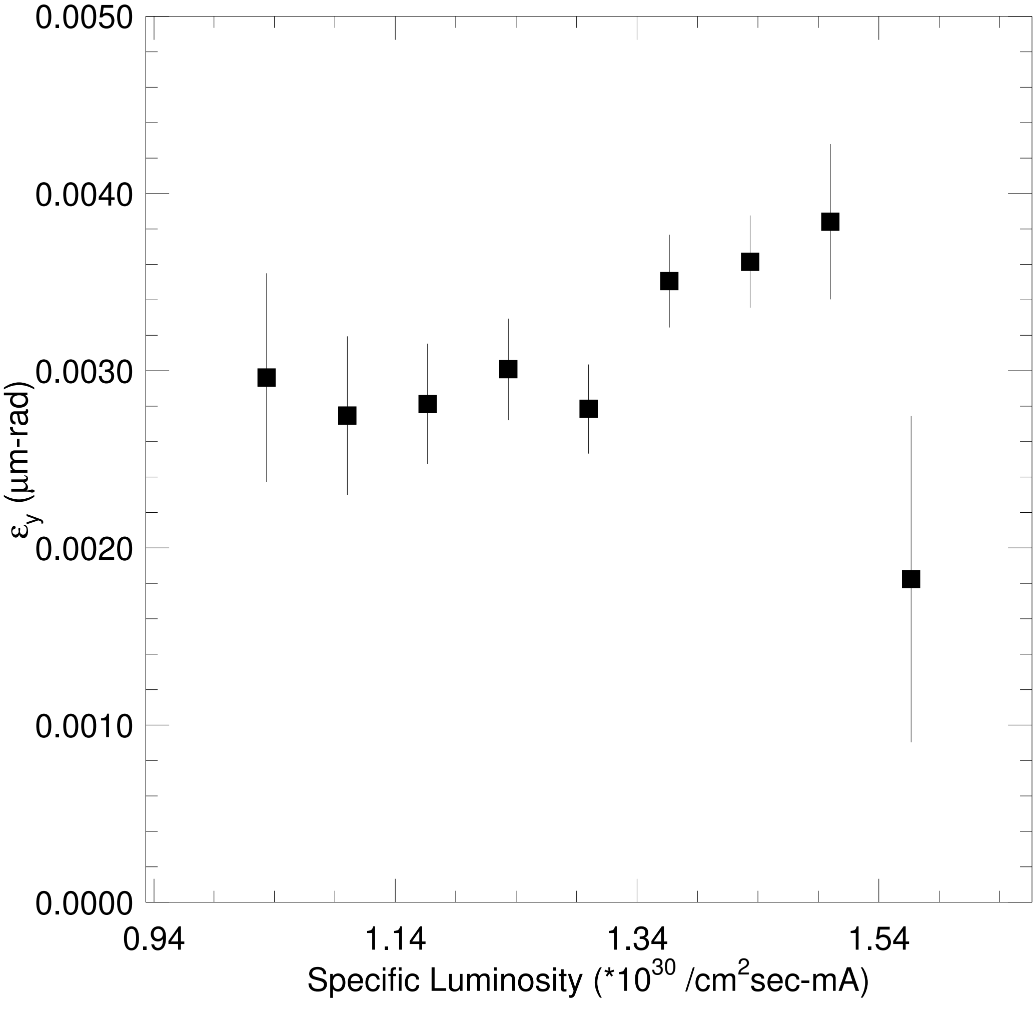

Figure 14: The extracted vertical emittance as a function of specific luminosity.

and assume a σ_x of 300μm and a β_y^* of 1.8cm. From these calculations we expect a β_x^* of 0.5m, an ϵ_x of 0.18μm-rad, and an ϵ_y of 0.0021μm-rad. We also expect a σ_y of 6.1μm. We measure a β_x^* of $(0.58 + 0.15 - 0.10)$m, an ϵ_x of 0.302$\pm$0.070 μm-rad, and an ϵ_y of 0.004$\pm$0.002 μm-rad. The agreement between our expectations and our measurements for this week are good. We also extract for that weeks running σ_x of 420$\pm$100 μm and a σ_y of 8.5$\pm$2.1 μm.

Another check was done Mike Billing [6]. He calculated vertical beam size and emittance as function of beam current based on the observed luminosity and expected dynamic effects on β_x, β_y, and ϵ_x for the same running period as our analysis. Figure 15 shows our results for the vertical emittance compared with Mike's analysis. Our measurement is clearly systematically larger than Mike's extraction. The agreement is better than it looks since Mike used fixed values without uncertainty for β_x, β_y, and ϵ_x. Including uncertainties and dynamic effects on these would expand the uncertainty on Mike's line by at least a factor of two. Mike also used his analysis to calculate a vertical beam size and gets results that span the range from 3 to 5 microns with a tail to higher values. Our measurement of ϵ_y, 0.0028$\pm$0.0010 μm-rad, combined with our previous measurement of β_y^* implies the vertical size of the beam at the interaction point is roughly 7.1$\pm$1.3 μm which does agree well with Mike's measurement of 4$\pm$1 μm. Again Mike's number only includes statistical uncertainty. Incidentally our measurement of the vertical size of the beam gives the vertical size of the luminous region, smaller than the single beam due to the overlap effect, to be 5.0$\pm$0.9 μm.

These two cross checks of our analysis give us confidence that our technique works well and within systematic uncertainties agrees with other methods.

Finally, we measured β_x^*, ϵ_x as functions of specific luminosity. The results are shown in Figure 16. We are unable to see any dynamic effects which we expect to be small for these parameters over this range of specific luminosity.

4 Another Application: Measurement of Energy Spread

The measurement of the energy spread of colliding beams is another task to which we apply the method described above. The momentum of a particle in the longitudinal direction, $\mathrm{p_z}$, is related to the energy spread of a beam, $\Delta\mathrm{E}$, so that

$$|p_z| = \mathrm{E_{beam}} \oplus \frac{\Delta\mathrm{E}}{\mathrm{E_{beam}}} \tag{8}$$

for the incoming beam particles. The colliding beams come from different directions and add incoherently. The sum of the momenta of colliding tracks over the beam energy in the longitudinal direction is a distribution with width $\sqrt{2}\Delta\mathrm{E}/\mathrm{E_{beam}}$. Thus we measure the "longitudinal peculiar momentum" in $e^+e^- \to \mu^+\mu^-$, $\sum \mathrm{p_z}/\mathrm{E_{beam}}$, and extract from this measurement the $\Delta\mathrm{E}/\mathrm{E_{beam}}$ for the colliding beams.

We study the longitudinal resolution with simulated samples of $e^+e^- \to \mu^+\mu^-$ 4SK and 4ST events. These events were generated with no beam energy spread, though we allowed for an energy spread from radiated photons and any other source. We observe a $\sum \mathrm{p_z}/\mathrm{E_{beam}}$ with a width of 10^{-6} in the resulting $\mu^+\mu^-$, and this is negligible as compared to our resolution which is of order 0.001. We guessed that this resolution depends on the longitudinal direction cosine, $|\cos\theta_z|$. We again binned our data according to SVX hit patterns and number of $Nhits$. To

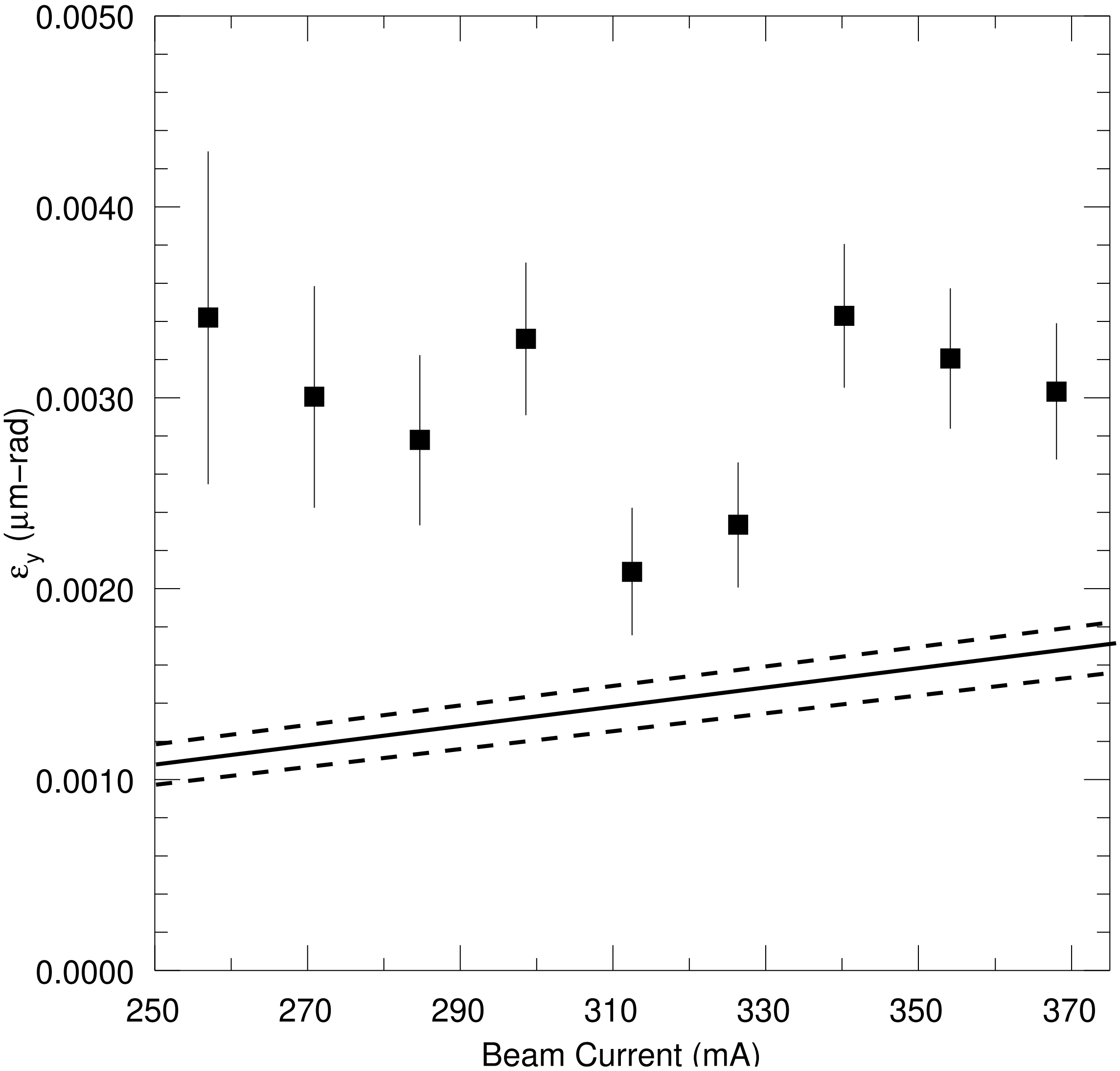

Figure 15: The vertical emittance as a function of beam current. Also shown is the central value and statistical uncertainty for the Mike Billing analysis discussed in the text.

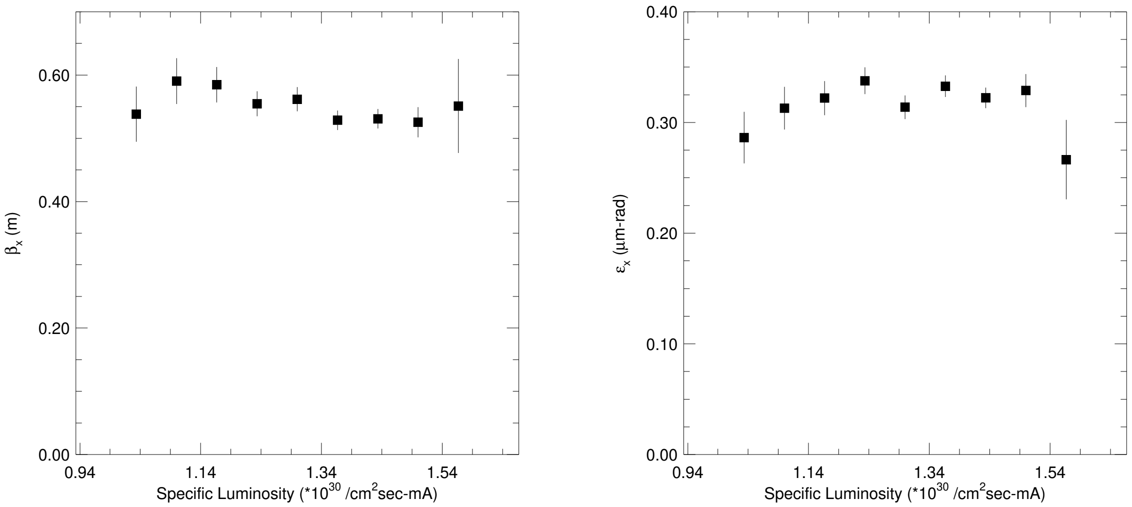

Figure 16: Horizontal beta and horizontal emittance as functions of specific luminosity.

ensure good statistics, we chose SVX hit patterns of (6,6) and (6,5) with more than 100 total tracking hits. For each subset we parametrized the resolution as

$$\text{Resolution} = m|\cos\theta_z| + b. \tag{9}$$

We fit a one dimensional distribution of the longitudinal peculiar momentum to this equation and extract the m and b values for each bin of SVX hit pattern and total number of tracking hits.

Figure 17 shows a comparison of the MC resolution to the real data for the 4ST dataset. For small $|\cos\theta_z|$ the observed increase of data over the resolution is as expected very small. Unfortunately for larger $|\cos\theta_z|$ our results do not make sense as the MC prediction for the resolution grows larger than the data. To resolve this discrepancy we looked for other drivers of the resolution. We considered the number of cathode hits, number of stereo hits, and azimuthal angle ϕ. We did not observe that the resolution effects of these were badly modeled by the simulation. Either the resolution had negligible dependence, ϕ, or the relative changes in resolution agreed well between the data and the simulation, number of cathode hits and stereo hits. Thus we could not resolve the discrepancy and we limit our data to $|\cos\theta_z| < 0.2$ when making this measurement, and these results on $\Delta\mathrm{E}/\mathrm{E}_{\mathrm{beam}}$ should be taken with a grain of salt.

To determine the energy spread of the beams, we fit real data projections of the longitudinal peculiar momentum in bins of $|\cos\theta_z|$ to a Gaussian with a width given by

$$\sqrt{(m|\cos\theta_z| + b)^2 + 2\left(\frac{\Delta\mathrm{E}}{\mathrm{E}_{\mathrm{beam}}}\right)^2} \tag{10}$$

In these fits, m, b, and $|\cos\theta_z|$ are fixed appropriately while the area, mean, $\sqrt{2}\Delta\mathrm{E}/\mathrm{E}_{\mathrm{beam}}$ and a flat background are floating. We then form a weighted average of the $\sqrt{2}\Delta\mathrm{E}/\mathrm{E}_{\mathrm{beam}}$, for all

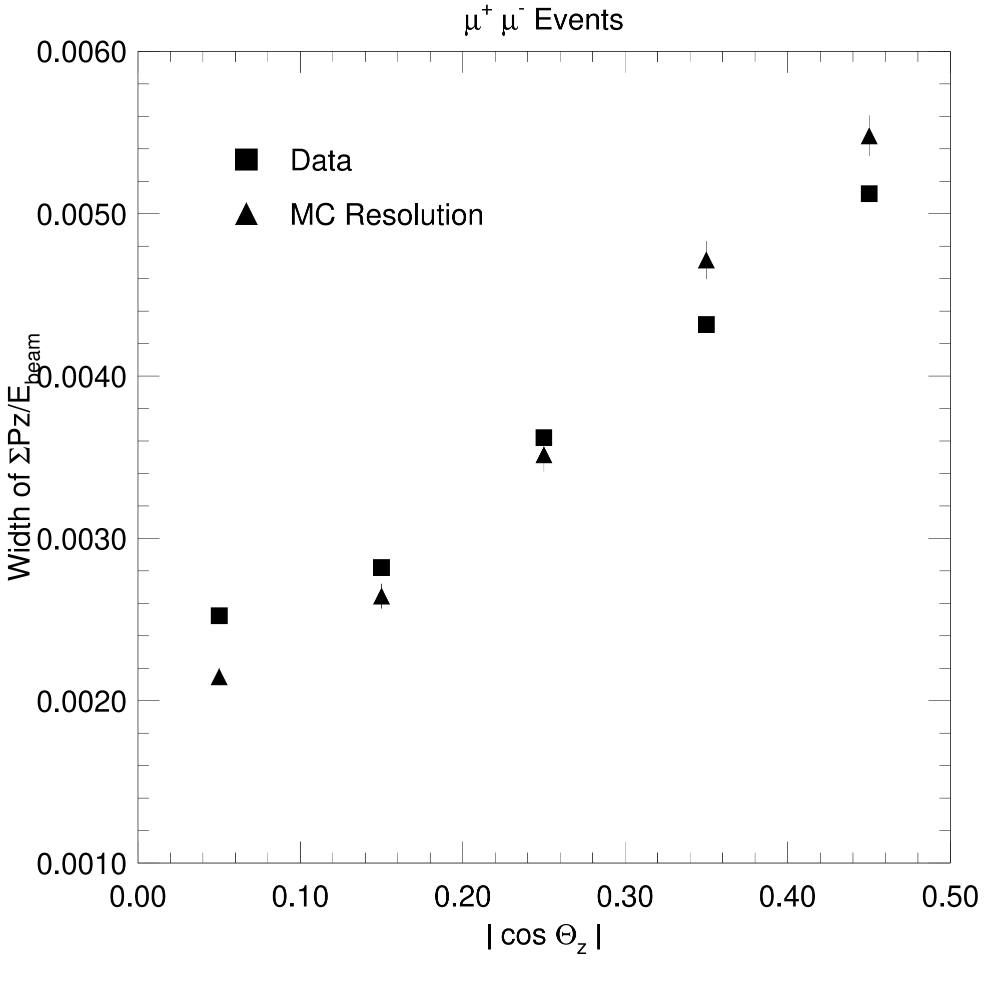

Figure 17: The sum of the longitudinal peculiar momentum as a function of the direction cosine for $Nhits$ of approximately 122 in the 4ST dataset.

Table 3: The values for the resolution parameters, m and b, for the three flavors of CLEO II.V resolution.

SVX Hit Pattern	$< Nhits >$	Resolution Model	$m \times 10^3$	$b \times 10^3$
(6,6)	113.5	4SK	3.1±1.5	1.89±0.13
(6,6)	113.5	Avg 4SK,4ST	4.4±1.5	1.86±0.14
(6,6)	113.5	4ST	5.7±1.5	1.83±0.15
(6,6)	122.0	4SK	2.5±1.3	2.04±0.12
(6,6)	122.0	Avg 4SK,4ST	3.5±1.1	1.93±0.11
(6,6)	122.0	4ST	4.5±1.0	1.82±0.10
(6,5)	113.5	4SK	4.5±1.9	1.86±0.22
(6,5)	113.5	Avg 4SK,4ST	5.4±1.8	1.89±0.39
(6,5)	113.5	4ST	6.3±1.7	1.92±0.16
(6,5)	122.0	4SK	3.2±1.6	2.08±0.18
(6,5)	122.0	Avg 4SK,4ST	3.6±1.7	2.02±0.17
(6,5)	122.0	4ST	4.0±1.7	1.96±0.16

$|\cos\theta_z|$, SVX hit patterns, and total tracking hits bins. The means are consistent with zero at the few times 10^{-4} level.

We made these measurements for all CLEO II.V datasets, except the 4SH. The 4SH dataset did not have enough statistics to make a measurement of the energy spread. The data is in three flavors of resolution: 4SH-4SK with nominal SVX hits and z weights bug; 4SL-4SN with improved SVX hits and z weights bug; and 4SP-4ST with improved SVX hits and no z weights bug. We have three sets of resolutions for each of these data sets. It is difficult to generate something with the bug. Fortunately, our 4SK MC is old and was generated with the bug. We therefore use the following resolutions for each data set. For the 4SH-4SK datasets, we use our 4SK resolution, for the 4SL-4SN datasets, we use average of 4SK and 4ST resolutions, and for the 4SP-4ST datasets, we use our 4ST resolution. We expect an energy spread, $\Delta\mathrm{E}/\mathrm{E}_{\mathrm{beam}}$, of approximately 0.000673 [7] for all CLEO II.V data.

We determine the systematic error on our measurements by varying the resolution parameters m and b as determined by the statistical error from a fit to the resolution from the simulations. These parameters and their errors are given in Table 3. Table 4 gives results of our data fits. The systematic errors on this measurement are rather large and our measured values are thus consistent with zero. We choose therefore to present the limit on the energy spread of the beam with a 90% C.L. in Table 5. These limits are consistent with the expectations of the CESR lattice.

5 Conclusions

We have developed a method to measure the angular distribution of the colliding beams in the luminous region of CESR at the CLEO interaction region. This method takes advantage of the very good hit resolution in the CLEO II.V SVX for $e^+e^- \to \mu^+\mu^-$ events. This resolution was found as a function of the number of tracking hits in the SVX, VD, and DR. Each SVX

Table 4: The measured energy spreads of CESR beams for all CLEO II.V datasets.

Dataset	Resolution Model	# Events	$\sqrt{2}\frac{\Delta E}{E_{beam}}$
4SH	4SK	419	N/A
4SJ	4SK	8155	$(0.00150\pm0.00011\pm0.00084)$
4SK	4SK	7973	$(0.00151\pm0.00010\pm0.00079)$
4SL	Avg 4SK,4ST	17405	$(0.00138\pm0.00008\pm0.00081)$
4SM	Avg 4SK,4ST	10420	$(0.00123\pm0.00009\pm0.00089)$
4SN	Avg 4SK,4ST	10190	$(0.00141\pm0.00010\pm0.00078)$
4SP	4ST	15546	$(0.00086\pm0.00009\pm0.00092)$
4SQ	4ST	7972	$(0.00083\pm0.00010\pm0.00072)$
4SR	4ST	7726	$(0.00100\pm0.00010\pm0.00080)$
4SS	4ST	20715	$(0.00084\pm0.00007\pm0.00096)$
4ST	4ST	25076	$(0.00080\pm0.00007\pm0.00094)$

Table 5: The limits on the energy spread of CESR beams at 90% C.L. for all CLEO II.V datasets.

Dataset	Limit on $\frac{\Delta E}{E_{beam}}$ (90% C.L.)
4SJ	0.0018
4SK	0.0018
4SL	0.0017
4SM	0.0017
4SN	0.0017
4SP	0.0015
4SQ	0.0013
4SR	0.0015
4SS	0.0015
4ST	0.0015

hit pattern was also found to have its own resolution function as well. This method, combined with the box method, allows us to make simultaneous measurements of the Gaussian width of the spatial spread of the beam and the Gaussian width of the angular spread of the beam. The simultaneous measurements allow us to extract the parameters β^*_x, ϵ_x and ϵ_y. β^*_y was previously measured and fixed to its constant value. The dynamic effects we had hoped to see for ϵ_x and ϵ_y were not visible, although the ϵ_y data are suggestive.

We also considered the beam energy spread with similar techniques. We found that the resolution of the z component of the momentum is not perfectly modeled by the simulation. We set limits on the beam energy spread of less than 0.2% at 90% C.L. in the CLEO II.V data that are consistent with the expectation from the CESR lattice.

References

[1] "First Measurement of $\Gamma(D^{*+})$ and Precision Measurement of $m_{D^{*+}} - m_{D^0}$", A. Anastassov *et al.* (the CLEO Collaboration), *Phys. Rev.* D65, (2002): 032003, CBX 01-23, D.Cinabro.

[2] CBX 00-22/CBN 00-6, D. Cinabro, K. Korbiak.

[3] "Novel Method of Measuring Electron Positron Colliding Beam Parameters", D. Cinabro, K. Korbiak, R. Ehrlich, S. Henderson, and N. Mistry, *Nucl. Instrum. Meth.* A481, (2002): 29-35.

[4] CBX 96-9/CBN 96-17 and CBX 97-39/CBN 97-14, D. Cinabro.

[5] CSN 96-347, A. Weinstein.

[6] `http://cesrelog.lns.cornell.edu/documents/progress/lum/results9899.html`

[7] Private communication from Dave Rubin.